Molecular beam epitaxy control of the structural, optical, and electronic properties of ScN(001)

Arthur R. Smith,[a] Hamad A. H. AL-Brithen, and David C. Ingram
Department of Physics and Astronomy, Ohio University, Athens, Ohio 45701

Daniel Gall
Coordinated Science Laboratory and Materials Research Laboratory, University of Illinois, 1101 West Springfield Avenue, Urbana, Illinois 61801

(Received 14 March 2001; accepted for publication 1 June 2001)

Scandium nitride (001) oriented layers have been grown on magnesium oxide (001) substrates by molecular beam epitaxy using a rf-plasma source and a scandium effusion cell. The Sc/N flux ratio is found to be critical in determining the structural, optical, and electronic properties of the grown epitaxial layers. A distinct transition occurs at the point where the Sc/N flux ratio equals 1, which defines the line between N-rich and Sc-rich growth. Under N-rich conditions, the growth is epitaxial, and the surface morphology is characterized by a densely packed array of square-shaped plateaus and four-faced pyramids with the terraces between steps being atomically smooth. The films are stoichiometric and transparent with a direct optical transition at 2.15 eV. Under Sc-rich conditions, the growth is also epitaxial, but the morphology is dominated by spiral growth mounds. The morphology change is consistent with increased surface diffusion due to a Sc-rich surface. Excess Sc leads to understoichiometric layers with N vacancies which act as donors. The increased carrier density results in an optical reflection edge at 1 eV, absorption below the 2.15 eV band gap, and a drop in electrical resistivity. © *2001 American Institute of Physics.*
[DOI: 10.1063/1.1388161]

I. INTRODUCTION

Transition metal nitrides are well known for their excellent physical properties including high hardness, mechanical strength, high temperature stability, and electronic transport properties that vary from semiconducting to metallic. Titanium nitride, the most studied transition metal nitride and which is used in optical and wear-resistant coatings, has a high hardness $H \sim 20$ GPa.[1–3] However, only a limited number of articles have been published on the growth and properties of ScN, which is also hard, $H \sim 21$ GPa,[2] and has a high melting point $T_m \sim 2600\,^{\circ}$C.[4] Yet the major interest in ScN is for its electronic properties. While early theoretical work suggested that ScN might be a semimetal,[5,6] early experimental work by Dismukes and more recently by several other groups have all shown that ScN has a direct optical transition in the range 2.1–2.4 eV.[2,4,7–10] In addition, recent theoretical work has shown that ScN is a semiconductor with a direct transition at the X point near 2.1 eV and a possible indirect transition from $\Gamma \rightarrow X$ at a lower energy in the range 0.9–1.6 eV.[11–13]

Further progress in understanding the properties of ScN requires detailed investigations of its crystal growth. The Sc–N bond is partially ionic,[14] which leads to its rocksalt crystal structure. In order to understand the growth of ScN, it is important to consider various possible crystalline orientations of the rocksalt structure. In the rocksalt structure, each Sc atom is bonded to six N atoms and each N atom is bonded to six Sc atoms with octohedral geometry. In the case of (111) oriented surfaces, each atom will have three dangling bonds pointing out of the surface. Indeed, while (111) oriented films have been reported by a number of groups, none have reported smooth growth, suggesting that a high surface diffusion barrier exists for (111) oriented surfaces.[8–10] By comparison, for the (001) bulk-terminated surface, each surface atom will be bonded to five neighbors, four in the surface layer and one in the second layer, thus leaving just a single dangling bond pointing out of the surface. There may therefore be a lower diffusion barrier on (001) compared to (111) oriented surfaces. Gall *et al.* reported (001) oriented ScN growth in the case of sputter deposition; however, in order to avoid the inclusion of (111) grains, it was necessary to apply a substrate bias resulting in incident N ions with energy about 20 eV.

Only two articles have reported the growth of ScN using molecular beam epitaxy (MBE).[8,15] Moustakas *et al.* grew ScN on sapphire(0001) using electron cyclotron resonance-MBE, resulting in polycrystalline films with highly preferred (111) orientation, consistent with the findings from other growth methods.[8] Recently, we reported the growth of ScN using rf-MBE.[15] For growth on sapphire (0001), we also obtained (111) orientation with a rough surface. Rough growth also occurred on MgO(110). For growth on MgO(001) on the other hand, we found that smooth, epitaxial films with (001) orientation were obtained, thus showing that the surface diffusion barrier on ScN(001) is indeed lower compared to ScN(111). Furthermore, since atomically smooth surfaces having terraces and well-defined step edges were obtained as shown by scanning tunneling microscopy (STM), the growth

[a]Electronic mail: smitha2@ohio.edu

mode is evidently two-dimensional, indicating fairly large surface diffusion lengths at the growth temperature we used — about 800 °C.

Although epitaxial growth of ScN has now been achieved, it is still not known how the growth and properties of the ScN(001) depend on the growth conditions such as substrate temperature and Sc/N flux ratio. An advantage of MBE growth over other methods like reactive sputtering or chemical vapor deposition is that it allows to controllably vary the Sc-to-N flux ratio over a wide range. Thus, here we report the strong effects of the Sc/N flux ratio on the growth mode, surface morphology, and optical and electrical properties of ScN(001) films. When the Sc/N flux ratio is less than 1 (N-rich conditions), we find smooth epitaxial films, indicating substantial surface adatom mobility. Excess N atoms recombine and desorb as N_2; thus, the resulting stoichiometry is 1:1, and we observe a direct optical transition near 2.15 eV. As the Sc/N ratio exceeds 1 (Sc-rich conditions), a Sc-rich surface structure is formed. This changes the diffusion barrier, resulting in a net increase in the surface mobility. This increased surface mobility completely changes the surface morphology to a much smoother surface. However, since the Sc desorption rate from the surface is negligible, defects, most likely N vacancies, are incorporated into the film, leading to understoichiometric films; these show degraded optical properties, including absorption below 2.15 eV and a reflection edge at 1 eV.

II. EXPERIMENTAL PROCEDURE

The ScN layers are grown by MBE on MgO(001), using a rf plasma source for nitrogen and an effusion cell for scandium. Substrate temperature is measured using a thermocouple located behind the substrate heater and also using an infrared pyrometer looking at the front side of the sample. The MgO(001) substrates are 1 cm×1 cm square and polished on the side where the ScN growth takes place. The samples are coated on the backside with titanium or molybdenum to absorb heat from the radiant substrate heater.

The growth procedure begins by cleaning the substrate using acetone and isopropanol. Then, after introducing the substrate into the growth chamber, it is heated at ~950 °C with the nitrogen plasma source turned on. After 30 min, the substrate temperature is lowered to ~800 °C, and the flow rate of nitrogen is set to 1.1 sccm. At this point, the MgO(001) substrates typically show streaky reflection high-energy electron diffraction (RHEED) patterns along both ⟨100⟩ and ⟨110⟩ directions. Using such starting templates, ScN growth begins.

To investigate how the growth depends on the flux ratio J_{Sc}/J_N, samples are grown at different Sc flux in the range $0.3–4.2\times10^{14}$ cm^{-2} s^{-1} by adjusting the temperature of the scandium effusion cell. The flux is determined by measuring the thickness of the sample using a thickness profilometer and then computing the growth rate by dividing by the total growth time. Multiplying the growth rate in Å s^{-1} by the number density of Sc atoms in ScN (4.39×10^{14} cm^{-2} Å^{-1}) yields the Sc flux in atoms cm^{-2} s^{-1}. The obtained growth rate is in excellent agreement with the Sc deposition rate measured using a quartz crystal thickness monitor located inside the growth chamber, and with the deposition rate as determined by measuring the sample thickness using optical methods.

For purposes of defining the Sc/N flux ratio, it is important to know the active nitrogen flux J_N. In an effort to maintain the same effective N flux for this study, samples were grown using the same rf plasma power=500 W. Background chamber pressure is set in the range $8–9\times10^{-6}$ Torr. It is difficult to measure directly the value of the active nitrogen flux at the sample position in the case of a nitrogen plasma source. Myoung *et al.*, who reported a flux ratio dependent study of GaN growth by rf MBE, defined the effective nitrogen flux as the incorporated N flux at the highest growth rate in their system.[16] Such a procedure is possible in the case of GaN because of the unique kinetics of GaN growth in which excess Ga actually reduces the growth rate, as reported by Held and co-workers.[26] However, in the case of ScN growth, we have not observed such a maximum growth rate. Instead, when J_{Sc} exceeds J_N, the growth rate continues to increase, resulting in nonstoichiometric growth. As we shall show, the value of J_{Sc} at which this occurs becomes quite clear upon examining the film properties.

Therefore, we define the active nitrogen flux as that which gives the highest growth rate of ScN resulting in stoichiometric films as determined by Rutherford backscattering and by examining the film properties. The active N flux J_N in our system is then the Sc flux at this transition point, which we refer to as $J_{Sc,t}$. In our system, this value of $J_{Sc,t}$ and thus the active N flux J_N is $\sim3.6\times10^{14}$ cm^{-2} s^{-1}. The flux ratio J_{Sc}/J_N is thus determined by dividing J_{Sc} by J_N.

The growth process is monitored in real time using RHEED. At the end of growth, the Sc shutter is closed and the N-plasma source is turned off at about the same time or shortly thereafter. After the sample cools down, it is transferred under ultrahigh vacuum to an adjoining surface analysis chamber where it is analyzed using *in situ* STM and Auger electron spectroscopy (AES). Finally, the sample is removed from the vacuum chamber where it is analyzed using atomic force microscopy (AFM), x-ray diffraction (XRD), Rutherford backscattering (RBS), spectrophotometry, and four-point probe measurement of the room-temperature resistivity. The RUMP program is used to analyze the RBS data.[17]

III. RESULTS AND DISCUSSION

A. Structural properties

The crystalline orientation of the ScN films is determined using XRD. The x-ray wavelength is that of Cu $K\alpha$; since we usually do not resolve $K\alpha1$ ($\lambda=1.5405$ Å) vs $K\alpha2$ ($\lambda=1.5443$ Å), we use an average value for λ of 1.542 Å. Figure 1 shows a typical XRD spectrum for ScN grown on MgO(001) using MBE. In this case, the Sc flux was 2.9×10^{14} cm^{-2} s^{-1}, which equates to a Sc/N flux ratio of 0.80. A typical XRD rocking curve (ω-scan profile) is shown in the inset. Similar XRD 2θ spectra are observed over a wide range of Sc/N flux ratio from 0.13 to 1.17. A correction is applied to the XRD spectrum so that the 002 peak of MgO is

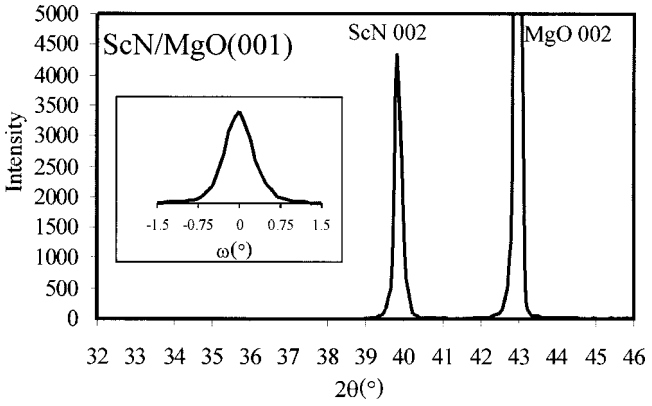

FIG. 1. 2θ x-ray diffraction spectrum for ScN film grown on MgO(001); inset shows typical ω rocking curve profile for the same sample.

shifted to 42.94°, in order to give the value found in tables for the MgO lattice constant of 4.213 Å.[18] Then for this sample we find the 002 peak of ScN at 39.84°, corresponding to a perpendicular lattice constant of $a_{\mathrm{ScN},\perp}=4.526$ Å. The measured value is a little larger than the expected bulk relaxed value of 4.501 Å.[7] This indicates the layer may not be completely relaxed and/or there may be a small amount of compressive strain due to cooling from the growth temperature. Since 002 is the only significant ScN peak seen, we find that the ScN films grown on MgO(001) substrates have a single orientation which is (001). Thus, rf MBE growth of ScN on MgO(001) is a reliable method to obtain (001)-oriented ScN layers, in contrast to growth by reactive magnetron sputtering which yields to a mixture of (001)- and (111)-oriented grains.[9]

In Fig. 2 are shown RHEED patterns for the MgO(001) substrate and four different ScN(001) films grown on MgO(001) substrates at different flux ratios. The images on the left are acquired with the RHEED beam normal to the square sample edge, and it is known that the directions perpendicular to the sample edges are $\langle 100\rangle$. The images on the right side of Fig. 2 are acquired with the sample rotated 45° in the azimuthal direction compared to the images on the left side, and are thus along $\langle 110\rangle$. Because of the fcc structure, the spacing between the rows of Sc atoms along $\langle 100\rangle$ is $a/2$, whereas the spacing between the rows of Sc atoms along $\langle 110\rangle$ is $a/\sqrt{2}$. Therefore, in reciprocal space the spacing between the primary diffraction lines for $\langle 100\rangle$ is $\sqrt{2}$ larger than the spacing along $\langle 110\rangle$. Since we do not observe any fractional order lines, the surface structure is 1×1 both during and after growth. The RHEED patterns are also equivalent under 90° rotations. Therefore, these films have fourfold symmetry as expected for the (001) face of the rocksalt structure and are thus epitaxial with the MgO(001) substrates with $[100]_{\mathrm{ScN}}\|[100]_{\mathrm{MgO}}$.

The Sc/N flux ratios for the films of Figs. 2(b), 2(c), 2(d), and 2(e) are 0.26, 0.8, 1.03, and 1.17, respectively. As seen in Fig. 2(b), for a flux ratio of only 0.26, the RHEED patterns along both directions are streaky but not totally smooth as seen by the nodes. While epitaxial growth occurs, the nodes correspond to some diffraction from the lattice perpendicular to the surface. This occurs when there exist

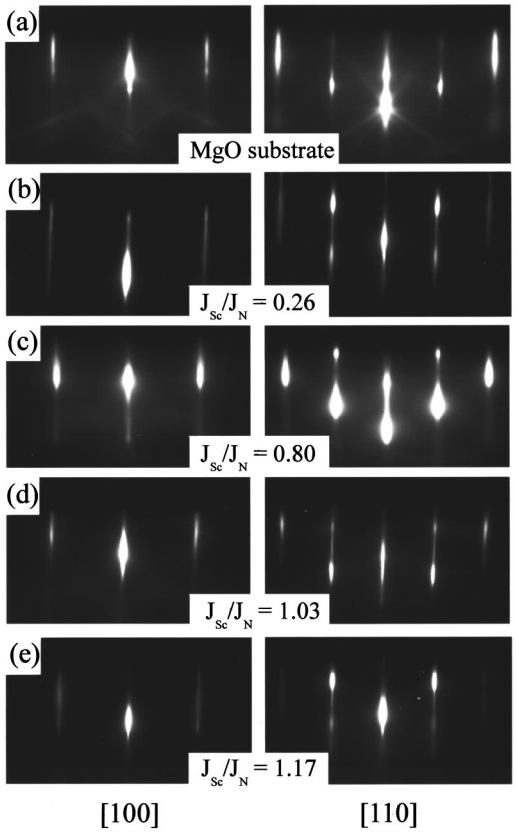

FIG. 2. RHEED patterns for (a) MgO(001) substrate and (b)–(e) ScN(001) layers as a function of Sc/N flux ratio with $J_{\mathrm{Sc}}/J_{\mathrm{N}}=0.26$, 0.80, 1.03, and 1.17.

some three-dimensional surface features. Since the ScN rocksalt lattice is just fcc with a two atom basis (Sc and N), the reciprocal lattice is bcc with a possible intensity modulation of the spots. Therefore, the nodes seen along $\langle 100\rangle$ correspond to reciprocal lattice points on the (100) face of the body-centered cube. Nodes seen along $\langle 110\rangle$ correspond to reciprocal lattice points on the (110) plane of the body-centered cube which slices through the center of the cube.

For flux ratio $J_{\mathrm{Sc}}/J_{\mathrm{N}}=0.8$, streaks are still present, but the nodes are brighter, indicating more three-dimensional features under N-rich conditions. However, for Sc/N flux ratio=1.03 (Sc-rich conditions), as seen in Fig. 2(d), the nodes are much weaker compared to Fig. 2(c). This shows that the three-dimensional structures corresponding to the nodes are reduced in size or in number on the surface for slightly Sc-rich conditions. We thus find that Sc-rich conditions result in smoother surfaces. Even for very Sc-rich conditions ($J_{\mathrm{Sc}}/J_{\mathrm{N}}=1.17$), the RHEED patterns are quite streaky as shown in Fig. 2(e).

To see how these RHEED patterns correlate with the surface morphology, we have performed AFM imaging on the same samples. Shown in Figs. 3(a), 3(b), 3(c), and 3(d) are AFM images of the same four ScN films grown using flux ratio $J_{\mathrm{Sc}}/J_{\mathrm{N}}=0.26$, 0.80, 1.03, and 1.17, respectively. The size of each image is 2 μm$\times$2 μm, and the images are oriented with sides parallel to [100] and [010] directions.

As seen in the AFM image of Fig. 3(a), for the sample grown at $J_{\mathrm{Sc}}/J_{\mathrm{N}}=0.26$ (very N-rich conditions), the surface

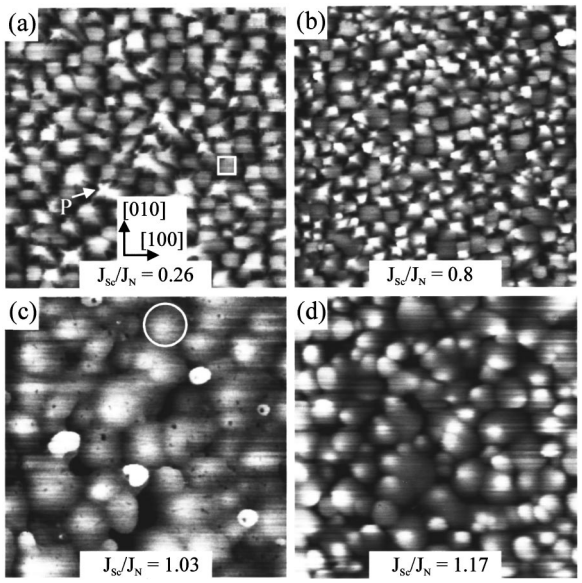

FIG. 3. AFM images of ScN films as a function of Sc/N flux ratio: (a) and (b) N-rich conditions; (c) and (d) Sc-rich conditions. Each image size is 2 μm$\times$2 μm.

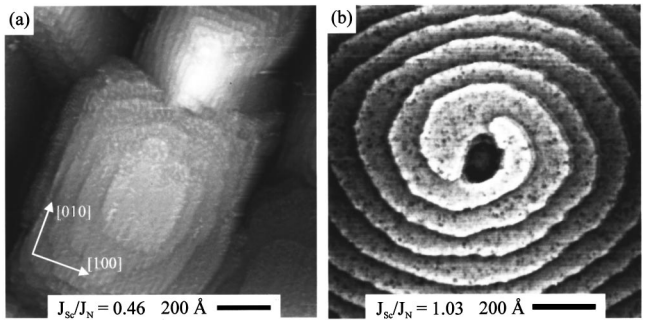

FIG. 4. STM images of ScN(001) surfaces: (a) N-rich growth surface. STM sample bias=-2.0 V, tunnel current=0.2 nA; (b) Sc-rich growth surface. Sample bias=2.0 V, tunnel current=0.2 nA.

is made up of many small mounds. While not all identical, close inspection reveals that many of these mounds have almost square shapes with flat tops; a typical flat-topped mound is outlined by a white square on the image. The square-shaped mounds have their sides along [100] and [010]. These square-shaped mounds are approximately 1200 Å$\times$1200 Å in lateral size and about 74 Å in maximum height (=gray scale range shown). The surface is thus very smooth (rms roughness only 19 Å), as also indicated by the streaky RHEED pattern shown in Fig. 2(b). Other mounds having a similar or slightly smaller size are pyramidal in shape. An example is indicated by *P* in the image. The pyramids are gently sloped, with apex angles of about 165°. The total density of both types of mounds is about 40 mounds μm^{-2} of which there are about 10 pyramids μm^{-2}.

As seen in Fig. 3(b), for increased $J_{Sc}/J_N=0.80$, we find a similar surface morphology composed of both flat-topped and pyramidal-shaped mounds. The mound heights are very similar (gray scale range shown=86 Å, rms roughness =21 Å); however, the mound densities are higher. The total density of flat-topped and pyramidal mounds is about 70 mounds μm^{-2} of which there are about 30 pyramidal mounds μm^{-2}. This increased density of pyramidal mounds explains the increased node intensity seen in Fig. 2(c). Therefore, the nodes seen in the RHEED patterns for N-rich conditions [Figs. 2(b) and 2(c)] are a consequence of diffraction through the pyramidal-shaped mounds, which are the three-dimensional surface structures. We thus observe increased pyramid density with increased Sc/N flux ratio in N-rich conditions.

As shown by the AFM image in Fig. 3(c), as the growth becomes Sc-rich ($J_{Sc}/J_N=1.03$), we find distinctly different surface morphology. In place of the square and pyramidal-shaped mounds, the Sc-rich grown film shows smoother, rounded mounds; a typical rounded mound is outlined by a white circle on the image. These rounded mounds have typical diameters of 2000–3000 Å and have smaller height (gray scale range shown=52 Å, rms roughness=11 Å). In addition, the mound density is only about 10 rounded mounds μm^{-2}. Compared to N-rich grown films, there are 4–7 times fewer mounds μm^{-2} which are also nearly two times smaller in height. Fewer and shorter mounds correspond to a smoother surface which correlates with the streakier RHEED patterns shown in Fig. 2(d). Even at very high Sc/N flux ratio=1.17, shown in Fig. 3(d), the surface morphology still consists of smooth rounded mounds.

To examine these surfaces with atomic-scale resolution, *in situ* STM has been performed. Shown in Fig. 4(a) is a STM image of a sample grown under N-rich conditions ($J_{Sc}/J_N=0.46$). This image shows a zoom-in view of one of the square, flat-topped mounds ~800 Å across and one of the pyramidal-shaped mounds. Individual atomic steps separating smooth terraces are observed. The atomic steps are generally along [100] and [010] directions. The terraces on the pyramidal mound are very narrow compared to those on the flat-topped mound but also along [100] and [010] directions. We attribute the pyramidal mounds to growth around screw-type dislocations in the film. Assuming one dislocation per pyramid, we estimate the dislocation density to be in the range $1\times10^9-3\times10^9$ cm^{-2} for our samples grown under N-rich conditions.

In Fig. 4(b) is shown a zoom-in STM image of a sample surface grown at $J_{Sc}/J_N=1.03$. This image shows that these rounded mounds are in fact large growth spirals. The growth spirals completely dominate the ScN surface morphology under Sc-rich growth conditions. Two single bilayer height steps (2.25 Å) emanate from the center of the spiral; therefore, the spiral is centered on a dislocation having a screw component of the Burger's vector equal to 4.50 Å (the ScN lattice constant) and pointing in the [001] direction. Every mound on these surfaces has at least one dislocation at the center. In addition, we also find other dislocations not at the mound centers. Therefore, the dislocation density calculated from the number of mounds is 1×10^9 cm^{-2}, but including all dislocations, not just those at mound centers, we estimate from other STM images as many as 1×10^{10} cm^{-2} for the Sc-rich grown film.

We have shown that dislocations cause pyramid growth in the case of N-rich conditions and round spiral growth in the case of Sc-rich conditions. We now consider the reason

why we observe this difference. For a constant substrate temperature, there are three important factors affecting film morphology - deposition rate, desorption rate, and diffusion rate. As the AFM images of Fig. 3 illustrate, we observe a major change in the morphology with only a small change in the deposition rate. Moreover, as Sc/N flux increases, we observe a linearly increasing growth rate which suggests that there is very little desorption. Therefore, since the substrate temperature is held approximately constant, the most probable explanation for the change in morphology is a qualitative change in surface diffusion.

The ratio of the diffusion length under N-rich conditions, $L_{\text{N-rich}}$, to that under Sc-rich conditions, $L_{\text{Sc-rich}}$, can be estimated by comparing the terrace width for the pyramidal mound to that for the spiral mound. For the pyramidal mound shown in Fig. 4(a), the terrace width is ~30 Å, whereas for the spiral mound of Fig. 4(b), the terrace width is ~110 Å. This is about a 4× increase in terrace width for Sc-rich conditions compared to N-rich conditions. Assuming that the diffusion length is proportional to the terrace width, the ratio $L_{\text{Sc-rich}}/L_{\text{N-rich}} \sim 4$. We attribute this increased diffusion length to a qualitative change in the Sc/N surface stoichiometry.

The well-ordered 1×1 reconstruction on one of the flat-topped mounds occurring under N-rich growth conditions has been atomically resolved by STM (shown elsewhere).[15] Calculations by Takeuchi show that a slight relaxation of the surface atoms of the bulk-terminated surface occurs, with the Sc atoms being displaced downward by about 0.03 Å compared to the N atoms.[19] Therefore, under N-rich conditions, the stable surface is nearly bulk-like. Under Sc-rich growth conditions, RHEED, XRD, and RBS channeling all show that the NaCl-structure is maintained. Yet close inspection of the STM image of the ScN surface in Fig. 4(b) shows a qualitatively different surface in which we do not observe any well-ordered reconstruction as we do for N-rich surfaces. For these STM tunneling conditions, the surface appears mostly flat and featureless, aside from some nanometer-sized pit features. This weak contrast strongly suggests a surface with metallic character. We infer that it is likely the surface has much more than just a few percent additional Sc. Calculations are underway to show an energetically favorable Sc-rich surface structure model, such as a single Sc adlayer.[19,20]

If such a Sc-rich surface structure exists, it could result in a decreased surface diffusion barrier due to weaker metallic Sc-Sc bonding. From our estimate of the increase in surface diffusion length (earlier), we can calculate the approximate change in the surface diffusion barrier using the well-known Arrhenius law[21]

$$N = \omega_A e^{-E_o/k_B T}, \tag{1}$$

where N is the average number of hops per unit time interval, ω_A is the atomic oscillation frequency (attempt frequency), and E_0 is the surface diffusion barrier. The diffusion length L is proportional to the square root of N. Assuming that the diffusion hop length and the attempt frequency are independent of surface composition, we obtain the following expression for the difference in the diffusion barriers $E_{\text{N-rich}}$ and $E_{\text{Sc-rich}}$ for N- and Sc-rich conditions

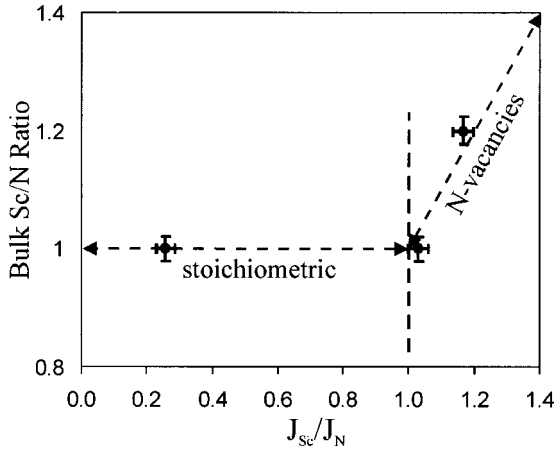

FIG. 5. Incorporated Sc/N concentration calculated from RBS data as a function of $J_{\text{Sc}}/J_{\text{N}}$.

$$E_{\text{N-rich}} - E_{\text{Sc-rich}} = 2k_B T \ln \frac{L_{\text{Sc-rich}}}{L_{\text{N-rich}}}. \tag{2}$$

For our typical growth temperature of 800 °C (1073 K), we thus calculate the difference in surface diffusion barriers to be about 0.26 eV.

Increased diffusion length due to a change in surface structure under Sc-rich conditions would explain the crossover from plateau-pyramid to rounded spiral morphology. Another question is whether the excess Sc on the surface will desorb back into the vacuum or incorporate into the film. To check the Sc/N bulk composition ratio of our samples, we performed Rutherford backscattering on three samples grown at different flux ratios. The RBS spectra are then analyzed and simulated using the RUMP code. Figure 5 shows the results of the RBS RUMP computations of the incorporated Sc/N ratios plotted versus the incident flux ratios. As is seen, the incorporated ratio is equal to 1.00 ± 0.02 for $J_{\text{Sc}}/J_{\text{N}} = 0.26 \pm 0.03$. This indicates that excess N atoms are not incorporated under N-rich growth conditions. The RBS result also shows that $\text{Sc/N} = 1.00 \pm 0.02$ for $J_{\text{Sc}}/J_{\text{N}} = 1.03 \pm 0.03$ (slightly Sc rich). Although we expect a slight deviation from 1:1 stoichiometry for this sample, this is near the limit of the RBS uncertainty. However, for incident flux ratio $J_{\text{Sc}}/J_{\text{N}} = 1.17 \pm 0.03$ (very Sc rich), the RBS result shows that $\text{Sc/N} = 1.20 \pm 0.02$. We conclude that for Sc-rich conditions, the incorporated Sc/N ratio is equal to the incident Sc/N flux ratio (within uncertainty).

Since RHEED, XRD, and also RBS channeling (not presented) all show that ScN films grown under Sc-rich conditions are of high crystalline quality, the off-stoichiometry must be explained by the existence of various point defects. Possibilities could include Sc-on-N-site (Sc_N) antisite defects or Sc interstitials; however, since these could lead to local metallic bonding with different structure (i.e., Sc metal is hexagonal), we would expect substantial degradation of the NaCl crystal structure, which we do not see even for the highest flux ratio. We therefore think that a more plausible explanation is the formation of N vacancies. NaCl-structure transition metal nitrides are known to exhibit large single

phase fields; thus they can sustain large vacancy concentrations. For example, TiN is stable in the NaCl structure for N/Ti ratios ranging from 0.6 to 1.2.[22]

B. Optical and electrical properties

As with the structural properties, the optical properties of ScN layers are found to be critically dependent on the Sc/N flux ratio. In this section, we describe how these properties vary with J_{Sc}/J_N. We find that although the films grown under Sc-rich conditions have smoother overall morphology, we also observe significant changes in the optical and electrical properties. In particular, we will show that the incorporated defects have a major effect on the reflection, transmission, and absorption coefficients of the film.

For samples grown under N-rich conditions, holding them up to a white light one observes an orange-red color, and the sample is very transparent. On the other hand, samples grown under Sc-rich conditions are darker in appearance. To make a quantitative comparison, we have measured the reflection and transmission coefficients, R and T, for ScN layers grown using different Sc/N flux ratios using spectrophotometry. Then the absorption coefficient α was calculated from R and T using a method described elsewhere.[9] In Fig. 6 are shown representative sets of data.

For the sample seen in Fig. 6(a) which was grown under N-rich conditions ($J_{Sc}/J_N=0.26$), R and T both show big oscillations due to multiple reflections at the interfaces. For $h\nu<2.1$ eV, R oscillates in the range 0.1–0.5, but then R levels out to about 0.3 for $h\nu>2.1$ eV. For $h\nu<2.1$ eV, T also oscillates in the range 0.4–0.8, but then T drops off sharply for $h\nu$ near 2.1 eV. Similar behavior to that shown here is observed for all samples grown under N-rich conditions.

Near $h\nu=2.1$ eV, where T drops off, we observe an increase in the absorption α up to about 3×10^5 cm^{-1}. Below 2.1 eV, α falls off to very small values and is essentially flat. If the absorption threshold near 2.1 eV corresponds to a direct band gap, the quantity $(h\nu\alpha)^2$ should be a linear function of $h\nu$. This plot is shown in Fig. 6(b) where it is seen that the data is indeed linear, strongly indicating that this threshold corresponds to a direct transition at the energy of 2.15 eV. No other absorption thresholds are observed down to 0.5 eV. If an indirect transition exists over the range of our measurement, it is below the sensitivity of our instrument.

The R and T spectra are substantially different for the films grown under Sc-rich conditions. As shown in Fig. 6(c) for the sample grown at a Sc/N flux $=1.17$, T is strongly reduced in the range 1–2 eV and shows almost no thickness oscillations. R also shows a strong reduction in its oscillations in the range 1–2 eV, and it exhibits a sharp reflection edge at 1 eV, where it increases from 0.15 at 1 eV to 0.7 at 0.5 eV. The direct absorption at 2.15 eV is still observed, but subbandgap absorption is also observed at the level of $0.3–0.5\times10^5$ cm^{-1}. Very similar results are also obtained for the sample grown at $J_{Sc}/J_N=1.03$.

We attribute the sharp reflection edge near 1 eV for the films grown under Sc-rich conditions to the existence of an increased number of free carriers compared to the samples

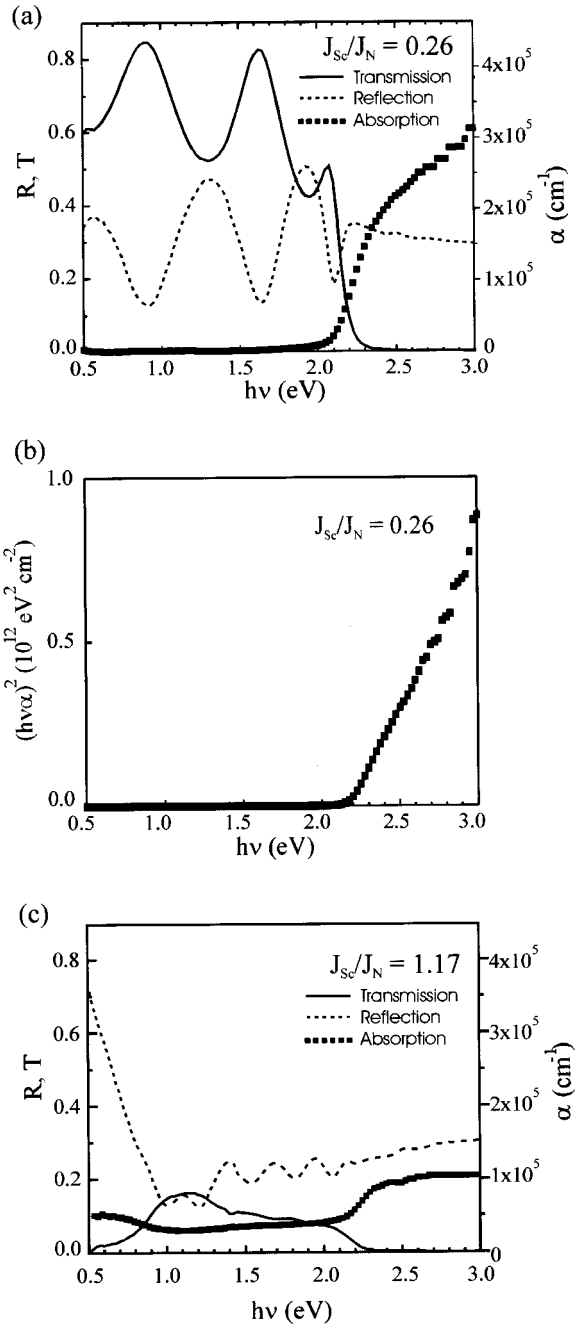

FIG. 6. Transmission, reflection, and absorption coefficients for ScN(001) films as a function of photon energy for (a) a sample grown under N-rich conditions with (b) the corresponding graph of $(h\nu\alpha)^2$ vs $h\nu$; and (c) a sample grown under Sc-rich conditions.

grown under N-rich conditions. Several recent articles have described the calculation of carrier concentrations and mobility from infrared reflectivity measurements in the case of GaN.[23,24] Fitting our ScN reflection spectrum with a Drude free electron gas model via a method described elsewhere,[25] we estimate the carrier density to be about 2×10^{21} cm^{-3} for samples grown under Sc-rich conditions.

One possibility is that the free carriers are coming from the N-vacancies acting as donors. For the sample grown with $J_{Sc}/J_N=1.03$, we would expect a carrier concentration of about 1.3×10^{21} cm^{-3}, in reasonable agreement with the value estimated from the Drude model fit. If all defects were

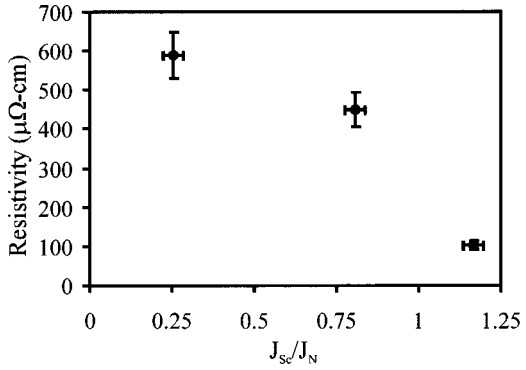

FIG. 7. Room temperature resistivity of several ScN(001) films as a function of J_{Sc}/J_N.

donors, the sample grown with $J_{Sc}/J_N = 1.17$ should have a carrier concentration of about 7.5×10^{21} cm^{-3}. This is almost 4× higher than the value from the Drude model fit, indicating that some compensating defects may occur at this very high Sc-flux.

Finally, we have also measured room-temperature resistivity as a function of Sc/N flux ratio. The results of this study are plotted in Fig. 7. Under N-rich conditions ($J_{Sc}/J_N=0.26$), the measured resistivity is 588 ± 60 $\mu\Omega$ cm. For $J_{Sc}/J_N=0.8$, the resisitivity decreases to 449 ± 40 $\mu\Omega$ cm. Then for Sc-rich conditions ($J_{Sc}/J_N=1.17$), the resistivity drops significantly to 103 ± 10 $\mu\Omega$ cm. This large drop in resistivity is explained by the increased carrier concentration.

C. Discussion and comparison to the case of MBE growth of GaN

In the N-rich growth regime, the growth rate of ScN is limited by the incident Sc flux since excess N atoms recombine and leave the surface as N_2. We have shown that such surfaces are still stable and that smooth, epitaxial, and stoichiometric films are obtained under this condition. These films are transparent with a direct optical transition at 2.15 eV. In the Sc-rich growth regime, where the Sc flux exceeds the N flux, the growth rate is still determined by the Sc flux since desorption of Sc from the ScN surface back into the vacuum is negligible. However, the excess Sc does not degrade the crystal structure or lead to amorphous growth as seen by the RHEED pattern which remain clear and streaky under Sc-rich growth conditions. We also find a smoother surface morphology in AFM images and excellent single crystal structure by RBS channeling. Even for flux ratio as high as 1.17, we still obtain excellent crystallinity.

Comparing to the case of MBE growth of GaN, in the N-rich growth regime the growth rate of GaN is also limited by the Ga flux.[26] N-rich conditions for GaN, however lead to a spotty transmission pattern in RHEED, indicative of a rough surface.[27,28] Several different groups have shown that Ga-rich growth conditions in MBE are favored for obtaining GaN with the smoothest surface.[27,29] The reason for smooth growth of GaN under Ga-rich conditions is that GaN surfaces are stabilized by the presence of one or more layers of Ga at the surface.[26,27,30,31] However, the excess Ga does not lead to nonstoichiometric growth. Held and co-workers showed that the excess Ga on the surface led to a Ga-rich surface layer but with the excess Ga re-evaporating back into the vacuum.[26] Smith and co-workers showed that the stable surface reconstructions occurring on both polar faces of wurtzite GaN contained one or more layers of Ga.[31–33] Tarsa and co-workers showed that Ga-rich conditions led to large round growth spirals, indicating that the diffusion length of adatoms is increased under Ga-rich conditions.[27] If the excess Ga layers are removed, however, the surface structure becomes unstable, resulting in rough growth.

We have shown that Sc-rich growth conditions also lead to large round growth spirals in the case of ScN growth. We have explained this is due to increased adatom diffusion length under Sc-rich conditions. However, since re-evaporation of Sc into the vacuum is negligible, Sc-rich conditions also lead to nonstoichiometric growth, unlike the case of GaN. A reason for this is the fact that the vapor pressure of Sc metal at the growth temperature of 800 °C (3×10^{-8} Torr) is much lower than that of Ga metal at 800 °C (6×10^{-6} Torr). Since the rocksalt structure is maintained, N vacancies are incorporated into the resulting film, and we observe a degradation of the optical properties, including subbandgap absorption, reduced transmission, and a reflection edge near 1 eV. Hence, while Ga-rich conditions may be preferable for GaN growth, N-rich conditions are clearly preferable for ScN growth by rf–MBE for the conditions described here.

IV. SUMMARY

We have grown ScN on MgO(001) substrates by rf–MBE and investigated how their structural, optical, and electrical properties depend on the Sc/N flux ratio during growth. We find (001) orientation for all flux ratios. RHEED patterns obtained during growth show that the surface is epitaxial under N-rich conditions and that the surface morphology is dominated by flat-topped and pyramidal shaped mounds. For Sc-rich conditions, the growth is also epitaxial, but the surface morphology is distinctly smoother and is dominated by round spiral mounds. The transition to spiral mound growth morphology is explained by an increased diffusion length of adatoms when the surface becomes Sc rich. Candidate Sc-rich model structures are currently being investigated.

The XRD and RHEED observations correlate well with changes in the surface morphology as measured by *in situ* STM and *ex situ* AFM. The excess Sc flux during Sc-rich growth leads to an increased growth rate which involves most likely the incorporation of N vacancies. This conclusion is supported by RBS measurements which show that the incorporated Sc/N ratio is equal to (within uncertainty) the incident Sc/N flux ratio for $J_{Sc}>J_N$. In addition, optical transmission and reflectivity measurements show very high reflectivity for photon energies in the range 0.5–1 eV and significant absorption below the bandgap in the range 1–2 eV, consistent with an increased carrier concentration.

On the other hand, for $J_{Sc}<J_N$, the incorporated Sc/N ratio measured by RBS is equal to 1. For these films, we find

an optical absorption edge corresponding to a direct transition at 2.15 eV. ScN therefore attains its best structural and optical properties when grown under N-rich conditions.

ACKNOWLEDGMENTS

This work has been supported by the Office of Naval Research and the National Science Foundation (Grant No. 9983816). The authors thank M. Kordesch for many useful discussions and F. Perjeru for help in coating substrates. The authors also thank S. Ulloa and N. Takeuchi Tan for useful discussions. Funding by the W. M. Keck Foundation is gratefully acknowledged.

[1] S. Yang, D. B. Lewis, I. Wadsworth, J. Cawley, J. S. Brooks, and W. D. Munz, Surf. Coat. Technol. **131**, 228 (2000); K. Inumaru, T. Ohara, and S. Yamanaka, Appl. Surf. Sci. **158**, 375 (2000).
[2] D. Gall, I. Petrov, N. Hellgren, L. Hultman, J. E. Sundgren, and J. E. Greene, J. Appl. Phys. **84**, 6034 (1998).
[3] H. Ljungcrantz, M. Odén, L. Hultman, J. E. Greene, and J.-E. Sundgren, J. Appl. Phys. **80**, 6725 (1996).
[4] X. Bai, Doctoral Dissertation, Ohio University, November 2000; X. Bai and M. E. Kordesch, Appl. Surf. Sci. **175–176**, 499 (2001).
[5] R. Monnier, J. Rhyner, T. M. Rice, and D. D. Koelling, Phys. Rev. B **31**, 5554 (1985).
[6] T. Eibler, M. Dorrer, and A. Neckel, Theor. Chim. Acta **63**, 133 (1983).
[7] D. Gall, I. Petrov, P. Desjardins, and J. E. Greene, J. Appl. Phys. **86**, 5524 (1999).
[8] T. D. Moustakas, R. J. Molnar, and J. P. Dismukes, Electrochem. Soc. Proceedings 96-11, 1996, p. 197.
[9] D. Gall, I. Petrov, L. D. Madsen, J.-E. Sundgren, and J. E. Greene, J. Vac. Sci. Technol. A **16**, 2411 (1998).
[10] J. P. Dismukes, W. M. Yim, and V. S. Ban, J. Cryst. Growth **13/14**, 365 (1972).
[11] D. Gall, M. Städele, K. Järrendahl, I. Petrov, P. Desjardins, R. T. Haasch, T.-Y. Lee, and J. E. Greene, Phys. Rev. B **63**, 125119 (2001).
[12] R. L. Lambrecht, Phys. Rev. B **62**, 13538 (2000).
[13] C. Stampfl, W. Mannstadt, R. Asahi, and A. J. Freeman, Phys. Rev. B **6315**, 5106 (2001).
[14] We calculated ScN to be ~18% ionic by setting a linear combination of ionic and covalent radii equal to the known lattice constant of ScN, 4.501 Å.
[15] H. A. Al-Brithen and A. R. Smith, Appl. Phys. Lett. **77**, 2485 (2000).
[16] J. M. Myoung, Q. Gluschenkov, K. Kim, and S. Kim, J. Vac. Sci. Technol. A **17**, 3019 (1999).
[17] L. R. Doolittle, Nucl. Instrum. Methods Phys. Res. B **9**, 344 (1985).
[18] The value for $a_{MgO}=4.213$ Å is from the Inorganic Index to Powder Diffraction (Joint Committee on Powder Diffraction Standards, International Center for Powder Diffraction Data, Swarthmore, PA, 1997): MgO (Card No. 04-0820). In our earlier paper [Al-Brithen *et al.*, Appl. Phys. Lett. **77**, 2485 (2000)], we had used 4.195 Å for a_{MgO}; using 4.213 Å in that letter, calculated values for $a_{ScN,\perp}$ would increase by about 0.02 Å.
[19] N. Takeuchi (unpublished).
[20] C. Stampfl (unpublished).
[21] A.-L. Barabási and H. E. Stanley, *Fractal Concepts in Surface Growth* (Cambridge University Press, Cambridge, 1995), p. 133.
[22] J.-E. Sundgren, B. O. Johansson, A. Rockett, S. A. Barnett, and J. E. Greene, *Physics and Chemistry of Protective Coatings*, edited by J. E. Greene, W. D. Sproul, and J. A. Thornton, American Institute of Physics Series Vol. 149 (AIP, New York, 1986), p. 149.
[23] J. A. Bardwell, M. W. C. Dharma-Wardana, H. Tang, and J. B. Webb, J. Vac. Sci. Technol. A **18**, 643 (2000).
[24] Z.-F. Li *et al.*, J. Appl. Phys. **86**, 2691 (1999).
[25] D. Gall, I. Petrov, and J. E. Greene, J. Appl. Phys. **89**, 401 (2001).
[26] R. A. Held, D. E. Crawford, A. M. Johnston, A. M. Dabiran, and P. I. Cohen, J. Electron. Mater. **26**, 272 (1997).
[27] E. J. Tarsa, B. Heying, X. H. Wu, P. Fini, S. P. DenBaars, and J. S. Speck, J. Appl. Phys. **82**, 5472 (1997).
[28] V. Ramachandran, C. D. Lee, R. M. Feenstra, A. R. Smith, J. E. Northrup, and D. W. Greve, J. Cryst. Growth **209**, 355 (2000).
[29] N. Grandjean and J. Massies, Mater. Sci. Eng., B **59**, 39 (1999).
[30] T. Zywietz, J. Neugebauer, and M. Scheffler, Appl. Phys. Lett. **73**, 487 (1998).
[31] A. R. Smith, R. M. Feenstra, D. W. Greve, J. Neugebauer, and J. E. Northrup, Phys. Rev. Lett. **79**, 3934 (1997).
[32] A. R. Smith, R. M. Feenstra, D. W. Greve, M.-S. Shih, M. Skowronski, J. Neugebauer, and J. E. Northrup, J. Vac. Sci. Technol. B **16**, 2242 (1998).
[33] A. R. Smith, R. M. Feenstra, D. W. Greve, M.-S. Shin, M. Skowronski, J. Neugebauer, and J. E. Northrup, Surf. Sci. **423**, 70 (1999).